Chapter 10

Investigating Stability and Finding New Solutions in Conservative Fluid Flows Through Bifurcation Approaches

10.1. Introduction

When considering the evolution of a fluid system, steady states can play a special role in characterizing the dynamics. Stable equilibria may be observed as long-lived structures, whereas unstable flows may play the role of attractors in the unsteady dynamics [DRI 95]. In fluid problems at sufficiently high Reynolds numbers, some portion of the flow domain may be approximately described by neglecting viscous effects (for a discussion of possible cases justifying this assumption, see, e.g., [BAT 67]). When this is possible, we may describe the flow through the Euler equations, which admit steady solutions without the need for external forcing. (It is important to note, however, that the form of the inviscid solution of interest is often determined by viscous considerations [BAT 56], and that the long-term dynamics may be affected by viscosity even in the absence of solid boundaries [LE 02].)

Historically, much of fluid stability theory has been developed around steady states that can be characterized analytically (e.g. [DRA 81, CRA 85]). However, analytical solutions to the Euler equations remain relatively rare. For this reason, a substantial amount of recent work has been focused on the numerical computation of steady Euler flows (e.g. [FLI 11, ELC 05]). This effort has been aimed mostly at flows of practical relevance, with applications including problems in geophysics [CAR 01], biological propulsion [DAB 09] and aircraft wakes [SAF 80]. The

---

Chapter written by Paolo LUZZATTO-FEGIZ and Charles H.K. WILLIAMSON.

Nonlinear Physical Systems: Spectral Analysis, Stability and Bifurcations
Edited by Oleg N. Kirillov and Dmitry E. Pelinovsky

accurate computation of these flows presents a number of subtle challenges. These include counting difficulties caused by degeneracies associated with the Hamiltonian structure of the problem [FLI 11], as well as the development of fine scales that may be difficult to resolve accurately [SAF 82].

For a numerically obtained fluid equilibrium, determining stability usually also requires a numerical (rather than analytical) approach [KAM 87, DRI 95]. This process is typically very sensitive to the resolution used in the stability calculation, and to the accuracy with which the steady solutions were initially computed [MEI 84, ELC 05].

An alternative approach to stability involves employing bounds based on conserved quantities (such as the energy) to establish that a perturbation cannot grow in time. These methods usually rely on computing the second variation of the energy (or of another conserved quantity) about the equilibrium, and examining whether this quantity is definite [HOL 85, MOF 85, DAV 98]. For example, it can be shown that a circular vortex is an energy maximum, and therefore admits only negative-energy modes (see [FUK 03]). However, for numerically obtained equilibria, the second variation of the energy can be prohibitively difficult to compute [DRI 85]. For this reason, indirect approaches to estimate the second variation of the energy can be valuable. Similarly, techniques yielding approximate eigenvalues for the linear stability problem can also prove useful. Such approaches may be used independently, or they could be employed to corroborate results from a linear stability analysis.

In this chapter, we highlight two such approaches. The application of these methodologies is illustrated by considering an example involving a family of steady flows comprising three corotating vortices. The stability of the basic flow has been recently considered in [LUZ 11b]. In this chapter, we establish the bifurcation structure for these equilibria.

10.2. Counting positive-energy modes from IVI diagrams

Here, we consider solutions of the Euler equations that are steady when observed in a moving reference frame. These solutions must satisfy:

$$\boldsymbol{u}_{\text{mov}} \cdot \nabla \boldsymbol{\omega} = \boldsymbol{\omega} \cdot \nabla \boldsymbol{u}_{\text{mov}} \quad [10.1]$$

$$\nabla \cdot \boldsymbol{u}_{\text{mov}} = 0, \quad [10.2]$$

where $\boldsymbol{u}_{\text{mov}}$ is the fluid velocity in the moving reference frame, and $\boldsymbol{\omega} = \nabla \times \boldsymbol{u}$ is the vorticity.

It is well established that such steady flows correspond to stationary points of the energy of the fluid, for given impulse, provided we consider only perturbations that are vorticity-preserving [SAF 92]. For example, for a rotating vortex configuration, a solution of [10.1] corresponds to a stationary point of the functional [SAF 92]:

$$H = E - \boldsymbol{\Omega} \cdot \boldsymbol{J}, \qquad [10.3]$$

where $\boldsymbol{\Omega}$ is the velocity of the moving frame, and the excess kinetic energy E and angular impulse $\boldsymbol{J}$ are defined as:

$$E = \frac{1}{2} \int \boldsymbol{\omega} \cdot \boldsymbol{A}\, dV, \quad \boldsymbol{J} = -\tfrac{1}{2} \int \boldsymbol{\omega} |\boldsymbol{x}|^2\, dV, \qquad [10.4]$$

where $\boldsymbol{A}$ is the vector potential satisfying $\boldsymbol{u} = \nabla \times \boldsymbol{A}$. The quantities E and $\boldsymbol{J}$ have an intuitive definition as the finite parts of the kinetic energy and angular momentum, respectively, in an unbounded flow (see [SAF 92] for a detailed discussion).

Since the first variation of H can be shown to be zero at equilibrium (that is, $\delta H = 0$; see, e.g., [SAF 92, FUK 08]), and H is conserved by the dynamics, the quantity $\delta^2 H$ can, in principle, be used to establish bounds on the growth of a perturbation. However, as mentioned in section 10.1, estimating $\delta^2 H$ for a numerically obtained equilibrium can be difficult. For this reason, there have previously been attempts to use a simple bifurcation diagram, for a family of steady flows, to extract information about $\delta^2 H$, by linking loss of definiteness with turning points in a control parameter [SAF 80, SAF 92]. However, a number of subsequent works pointed out several issues that remained to be addressed, and found counterexamples where this turning point approach gave incorrect stability predictions [DRI 85, DRI 95, LUZ 12a].

These issues can be briefly summarized as follows. First, while the bifurcation approach proposed in [SAF 80] is based on the assumption that a family of solutions has been computed, this methodology does not prescribe how such a solution family should be constructed. Since a fluid flow is an infinite-dimensional system, there are an infinite number of possible approaches to organize solutions into a one-parameter family [LUZ 12a]. Second, it is not clear how we should proceed in order to choose an appropriate control parameter, such that turning points in this parameter provide information about the stability of the flow [LUZ 12a]. Third, the bifurcation approach in [SAF 80] does not account for the presence of undiscovered bifurcations, which could lead to erroneous stability predictions [DRI 85, DRI 95].

By considering ideas from bifurcation theory [MAD 87], and introducing them to these fluid flow problems, [LUZ 12a] recently addressed these theoretical issues. This work showed that, if we construct solution families from vorticity-preserving

rearrangements, a bifurcation diagram provides information about the signature of $\delta^2 H$. It was numerically verified that, in an unbounded fluid, this condition leads to steady solutions that are organized along one-parameter families. Luzzatto-Fegiz and Williamson [LUZ 12a] also showed that the fluid impulse is an appropriate control parameter, such that turning points in impulse are linked with a change of signature for one mode. Furthermore, by plotting the frame velocity Ω and the impulse J for the solution family, we can infer whether a positive-energy mode is introduced or removed at the turning point in J, as shown in Figure 10.1. (This result will prove valuable in the example considered below.) This resolved the first and second issues noted above.

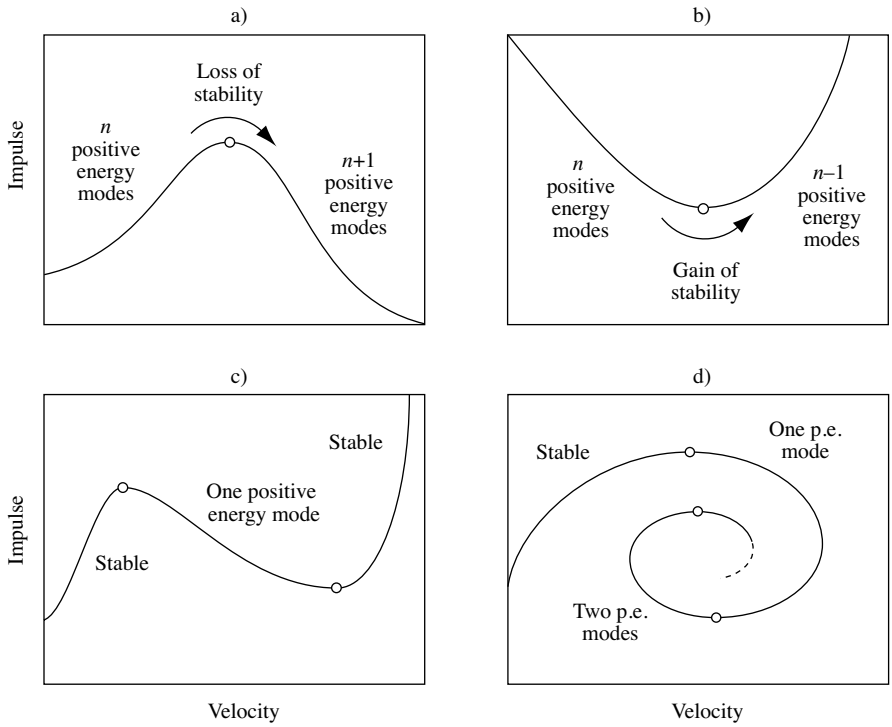

Figure 10.1. *Schematic plots illustrating the use of a velocity-impulse diagram to count the number of positive-energy modes*

The third problem, concerning the detection of bifurcations, was addressed as follows. [LUZ 12a] proposed introducing small "imperfections" in the flows, in the form of modifications that would break all geometric symmetries in the vorticity distribution. By computing the family of imperfect equilibria, we can break previously hidden bifurcations, and thereby uncover them. While this imperfection approach, for vortex flows, is not yet supported by rigorous proof, it has been

successful in detecting bifurcations in all examples that have been examined so far [LUZ 10, LUZ 12a, LUZ 12b].

On the basis of these developments, the properties of $\delta^2 H$ may be inferred from "Imperfect Velocity-Impulse (IVI) diagrams". Described algorithmically, determining stability by this approach requires performing the following steps:

1) Build a family of solutions from isovortical rearrangements.

2) For one member of the family, perform a complete linear stability analysis, and establish the signature of each eigenmode. This may reveal that $\delta^2 H$ is negative-definite, or that there exists a finite number of positive-signature eigenmodes.

3) Construct a velocity-impulse plot.

4) Introduce an imperfection that breaks all geometric symmetries in the vorticity distribution, and compute the imperfect solution structure.

5) As the solution family is traversed, use the turning points in impulse of the imperfect branches to count the number of positive-energy modes that are introduced, or removed.

6) Take the strength of the imperfection to zero and thereby recover the underlying bifurcation.

Of course, the number of positive-energy modes extracted from the "IVI diagram" approach provides an upper bound on the number of linearly unstable eigenmodes, and can therefore be employed as a simple check on the accuracy of a detailed linear stability analysis. In the next section, we outline how one may also approximately predict the onset of a resonant instability, for flows involving two-dimensional (2D) vortex equilibria.

10.3. An approximate prediction for the onset of resonance in 2D vortices

The appearance of a positive-energy mode does not, of course, imply that the flow must be linearly unstable. In some situations, the flow may initially remain linearly stable, and lose stability later, at a coalescence point of two purely eigenvalue pairs, as shown in Figure 10.2. After the collision, the eigenvalues may leave the imaginary axis, thereby giving rise to a complex quadruplet, which would correspond to a linearly unstable eigenmode (thereby yielding an oscillatory instability that grows exponentially [LAM 98]). Such instabilities (which we label as "resonances" in this chapter) are common in vortex dynamics. A classic example is presented by the development of the Kelvin–Helmholtz instabilities; this becomes apparent, for example, if we examine two streams with fixed densities, and consider the stability properties of a specific wave number as the velocity discontinuity is increased from a

small value (see, e.g., equation [16] in [DRA 70]). Another classic example is given by a subharmonic instability of the Kármán vortex street, if we examine the stability of a mode with fixed wave number, as the street aspect ratio is varied [MEI 84]. It should be emphasized that the definition of resonance employed here corresponds, in essence, to the existence of a linearly unstable mode with an oscillatory part (such that the higher order interaction between modes is not considered).

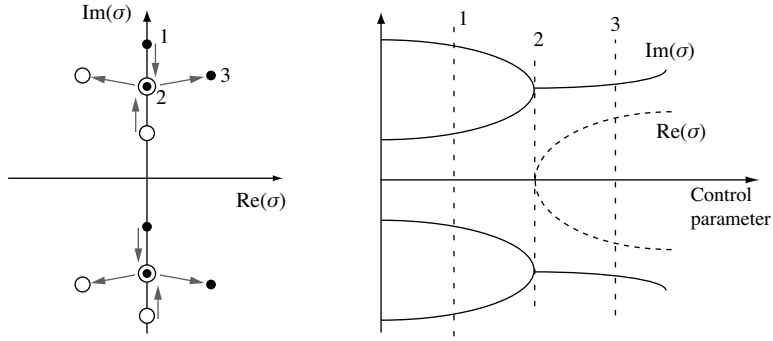

Figure 10.2. *Eigenvalue behavior for a Hamiltonian Hopf bifurcation (corresponding to a resonant instability, according to the definition used here). Perturbations are proportional to exp* (σt)*, such that Re* $(\sigma) \neq 0$ *corresponds to instability*

Luzzatto-Fegiz and Williamson [LUZ 11b] proposed that one may approximately predict the onset of resonance, in a vortex array, as follows. As noted earlier, solution families typically contain at least one member for which it is essentially trivial to compute linear stability eigenvalues, eigenmodes, and corresponding signatures. As also noted in the previous section, a typical unbounded vortex flow (with compact vorticity support) will reveal a countable infinity of negative-energy modes, and a finite number of positive-energy modes (as is indeed the case in the example below). Luzzatto-Fegiz and Williamson [LUZ 11b] proposed using an approximate model given by Moore and Saffman [MOO 71] to estimate the eigenvalues for each member of the solution family. Having also separately evaluated the signature for each eigenmode, Luzzatto-Fegiz and Williamson [LUZ 11b] showed that we can find the equilibrium for which opposite-signature (approximate) eigenvalues collided, thereby obtaining an approximate prediction for the onset of resonance.

According to this methodology, we may add the following step to the algorithm outlined in the previous section:

7) Employ the model of Moore and Saffman [MOO 71] to calculate approximate eigenvalues, and use signatures computed at step 2 to assess which eigenvalue collisions may yield a resonance.

Incidentally, we should note that, by construction, this last step does not shed additional light on problems where all solutions exhibit oscillatory instabilities, such that the main interest actually lies in the precise quantitative calculation of the eigenvalues, rather than in determining stability boundaries (as is the case, for example, for the stability of the family of Stuart vortices; see [PIE 82]). On the other hand, families of isolated, 2D vortex arrays often transition to instability through a resonance [DRI 85]; therefore, step 7 above is likely to provide useful information for these flows, as illustrated below.

10.4. An example: three corotating vortices

10.4.1. *Building a family of solutions from vorticity-preserving rearrangements*

Here, we consider a deceptively simple example, namely three equal-area, same-signed vortices in two dimensions. The vortices are modeled by regions with uniform vorticity ω and individual area A, each having circulation $\Gamma = \omega A$. Equation [10.1] then becomes:

$$\boldsymbol{u}_{\text{mov}} \cdot \boldsymbol{n} = 0 \qquad [10.5]$$

on the boundary of each vortex, where $\boldsymbol{n}$ is the unit normal to the contour. We solve [10.5] numerically using a procedure described in [LUZ 11a].

Since we are using a uniform vorticity approximation, the isovortical constraint is immediately satisfied provided that the area of each vortex is constant along the family. We introduce the non-dimensional quantities:

$$\Omega^* = \Omega\omega^{-1}, \quad J^* = J\,\Gamma_{\text{tot}}^{-2}\omega, \qquad [10.6]$$

where $\Gamma_{\text{tot}} = 3\Gamma$ is the total circulation. Equation [10.5] is solved using a numerical method described in [LUZ 11a]. The resulting family of solutions is shown later in Figure 10.3.

10.4.2. *Computing signatures for one member of the family*

Consider the flow involving three vortices whose separation distance L is much greater than the vortex mean radius a. Then two different descriptions of the flow may be adopted, depending on the dynamics of interest. From a global standpoint, the configuration will behave essentially as a collection of point vortices. On a local level, each vortex will be approximately circular, and therefore will support boundary

deformations that are well described by the eigenmodes of a circular vortex [THO 80]. We may therefore distinguish two different classes of eigenmodes: those associated with pure displacements of the vortices (as obtained from the point vortex viewpoint), and those corresponding to pure boundary deformations, which do not displace any of the vortex centroids. (Note that detailed linear stability analyses for vortex flows also support this decomposition; see, e.g., [DRI 85]). As noted in section 10.1, all eigenmodes for a circular vortex have negative signatures; therefore, in the limit $a/L \to 0$, all pure deformation modes have negative signature (see [LUZ 11b] for a detailed asymptotic analysis).

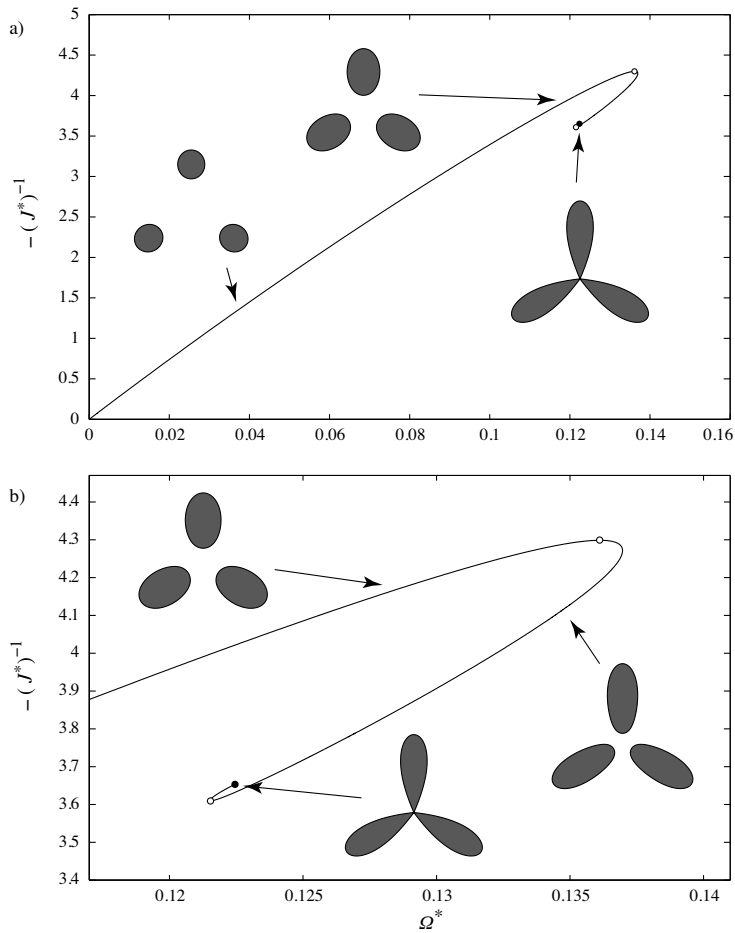

Figure 10.3. *Velocity-impulse diagram for three corotating, equal-area vortices. a) Overall view, b) closeup of the first two turning points*

Let us now consider in some detail the point-vortex approximation; then, it is easy to show that Ω is given by [ARE 09]:

$$\Omega = \frac{\Gamma}{2\pi L^2}. \qquad [10.7]$$

A point-vortex configuration is completely described by a finite-dimensional set of coordinates $\boldsymbol{\alpha}$ specifying the vortex positions [ARE 83]:

$$\boldsymbol{\alpha} = \begin{pmatrix} x_1 & x_2 & x_3 & y_1 & y_2 & y_3 \end{pmatrix}^T. \qquad [10.8]$$

Note that the isovortical condition is automatically satisfied if we consider perturbations that do not change the vortex circulations. Consider the linear stability problem obtained by perturbing the equilibrium configuration:

$$\boldsymbol{\alpha}_{\text{eq}} = L\begin{pmatrix} 1 & -\frac{1}{2} & -\frac{1}{2} & 0 & \frac{\sqrt{3}}{2} & -\frac{\sqrt{3}}{2} \end{pmatrix} \qquad [10.9]$$

to obtain:

$$\boldsymbol{\alpha} = \boldsymbol{\alpha}_{\text{eq}} + \varepsilon \Re\left\{\hat{\boldsymbol{\alpha}} \mathrm{e}^{\sigma t}\right\}, \qquad [10.10]$$

where $\varepsilon \ll 1$, and $\Re$ denotes real part. It is a classic calculation to solve the linear stability problem to find the following eigenvalues and eigenvectors [HAV 31]:

$$\begin{aligned}
&\sigma^{(1,2)} = 0, && \hat{\boldsymbol{\alpha}}^{(1,2)} = \begin{pmatrix} 0 & 1 & -1 & -\frac{2}{\sqrt{3}} & \frac{1}{\sqrt{3}} & \frac{1}{\sqrt{3}} \end{pmatrix}^T, \\
&\sigma^{(3,4)} = \pm \mathrm{i}\Omega, && \hat{\boldsymbol{\alpha}}^{(3,4)} = \begin{pmatrix} 1 & \frac{-1\pm \mathrm{i}\sqrt{3}}{2} & \frac{-1\mp \mathrm{i}\sqrt{3}}{2} & \pm\mathrm{i} & \frac{-\sqrt{3}\mp \mathrm{i}}{2} & \frac{\sqrt{3}\mp \mathrm{i}}{2} \end{pmatrix}^T, \\
&\sigma^{(5,6)} = \pm \mathrm{i}\Omega, && \hat{\boldsymbol{\alpha}}^{(5,6)} = \begin{pmatrix} 1 & 1 & 1 & \pm\mathrm{i} & \pm\mathrm{i} & \pm\mathrm{i} \end{pmatrix}^T.
\end{aligned} \qquad [10.11]$$

The second variation of H with respect to each eigenmode can be shown to be [LUZ 11b]:

$$\delta^2 H^{(1,2)} = 0, \quad \delta^2 H^{(3,4)} = \frac{3\Gamma^2}{2\pi L^2}\varepsilon^2 > 0, \quad \delta^2 H^{(5,6)} = \frac{3\Gamma^2}{2\pi L^2}\varepsilon^2 > 0. \qquad [10.12]$$

Therefore, we have that the configuration is linearly stable, yet appears to have two geometrically distinct, positive-energy eigenmodes, namely $(3,4)$ and $(5,6)$. However, as first recognized in [LUZ 11b], one of these eigenmodes plays no role in the stability problem. As a matter of fact, it can be shown that, for any general steady vortex flow, any mode corresponding to an overall displacement of the vortex configuration cannot take part in a resonance [LUZ 11b]. In this example, eigenmode $(5,6)$ can be recognized as an overall displacement mode. Therefore, there is effectively only one geometrically distinct positive-signature eigenmode.

10.4.3. *The velocity-impulse diagram*

The velocity-impulse diagram for the basic family of solutions is shown in Figure 10.3(a). Since $J^* \to -\infty$ as $\Omega^* \to 0$, we choose to plot $-(J^*)^{-1}$ instead. As seen clearly in Figure 10.3(b), the family of solutions traces a clockwise spiral; the turning points in impulse are labeled by open circles. We stopped the computations once the three vortices met at the center of the configuration; this final steady solution is marked by a black circle in Figure 10.3(b).

According to the turning point approach outlined in section 10.2, each of the open circles coincides with the introduction of a positive-energy mode, as one traverses the family starting from the solution involving well-separated vortices.

10.4.4. *Uncovering bifurcations by introducing imperfections*

To break all geometric symmetries in the vorticity distribution, we introduce small changes in the areas of the vortices, as shown in Figure 10.4. The area of vortex 2 in the figure is increased by 0.01%, whereas the area of vortex 3 is reduced by 0.01%. Note that while these changes are too small to be perceivable in this figure, these imperfections have an effect on the equilibrium calculations, which have an accuracy of at least six significant figures.

We consider three well-separated vortices, apply the imperfection and trace the resulting imperfect solution branch. After passing the first turning point in J^* (shown in Figure 10.3), we encounter a new turning point, after which the solutions rapidly diverge from the original family, thereby tracing the branch shown in the top-right half of Figure 10.5(a). As shown in this figure, this branch leads to a new family of solutions, whereby one vortex develops a corner while the others remain smooth.

To search for other bifurcations, we restart our calculations by taking another equilibrium on the basic branch (at a location past the bifurcation we just discovered) and computing more imperfect equilibria. This leads to the discovery of another solution branch (shown in the bottom-left quadrant in Figure 10.5(a). As shown by

the shape in the figure, this branch leads to an equilibrium such that two vortices approach each other and develop regions of high curvature, while the third vortex remains separated and smooth.

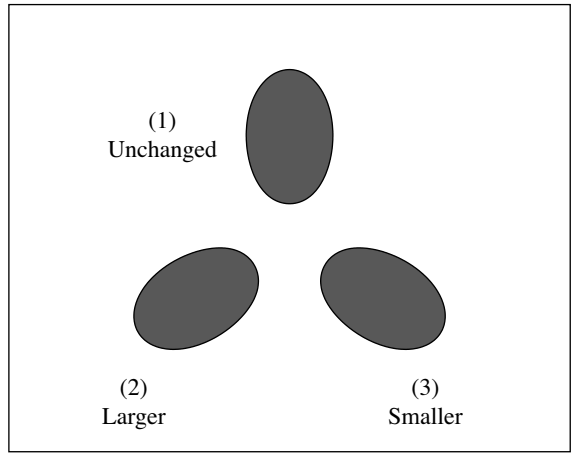

Figure 10.4. *The imperfection is constructed by breaking all geometric symmetries in the configuration. Here, we increase the area of vortex* (2)*, and reduce the area of vortex* (3)

We searched for further bifurcations along the original family, up to an equilibrium where the distance between the vortices and the origin is approximately 4% of the major axis of one vortex. We did not find any other bifurcations (although additional bifurcations are of course possible for solutions with smaller gaps between the vortices).

10.4.5. *Counting positive-energy modes from turning points in impulse*

We can use the turning points shown in Figure 10.3 and 10.5(a) to count the number of positive-energy modes; these are labeled as 1P, 2P, etc. Note that the curve in the top-right of Figure 10.5(a) traces an S-shaped path; we can therefore recognize that one positive-energy mode is introduced at the minimum of J^*, but another is removed at the following J^* maximum.

The turning point approach outlined in section 10.2 may also be applied to the other curve in Figure 10.5(a) to show that the "upper" portion must have one fewer positive-energy mode than the "lower" portion. In other words, if the lower branch has n positive-energy modes, the upper branch must have $n-1$ such modes. The value of n is found in the next section.

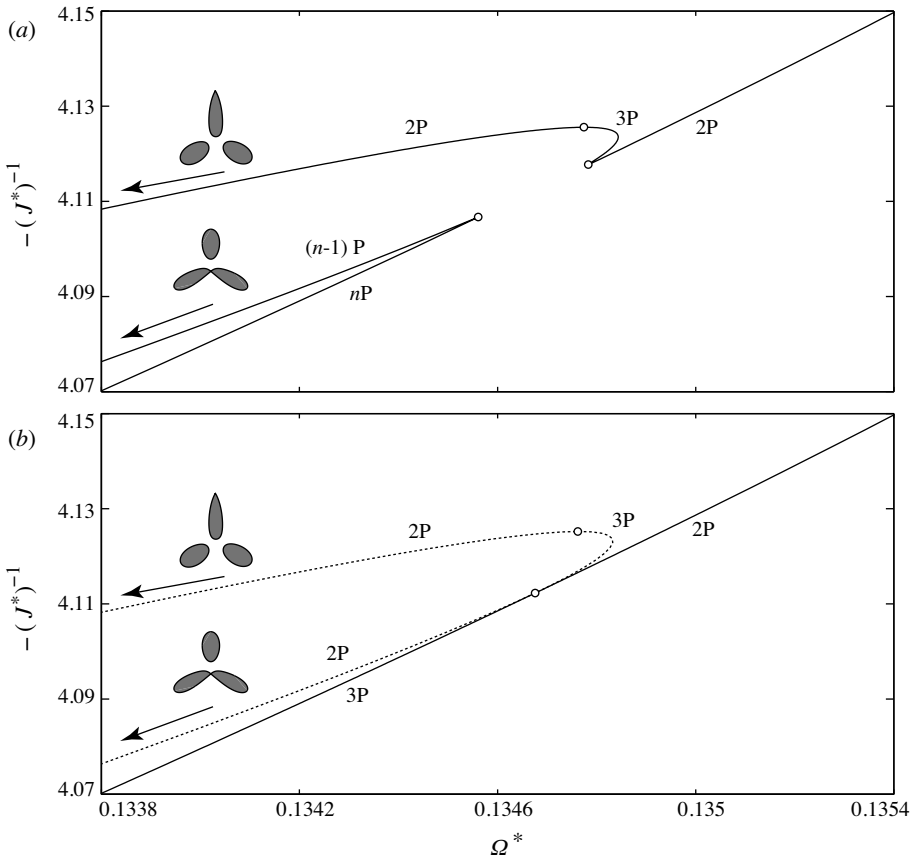

Figure 10.5. *Effect of introducing the symmetry-breaking imperfection. a) Detail of the imperfect velocity-impulse diagram, showing a broken bifurcation, which leads to two new solution branches. b) Underlying solution structure, recovered by removing the imperfection*

10.4.6. *Recovering the underlying bifurcation structure*

We now return the vortex areas to their original values, and recover the underlying bifurcation (shown in Figure 10.5(b), where the newly discovered solutions are accompanied by pictures of the associated limiting vortex shapes). Note that $n = 3$ is the only choice that enables us to traverse the bifurcation in any direction while losing or gaining at most one positive-energy mode. Therefore, we conclude that $n = 3$. An overall view of the resulting velocity-impulse diagram, including the new branches (shown by the dashed line), is shown in Figure 10.6(a) and (b).

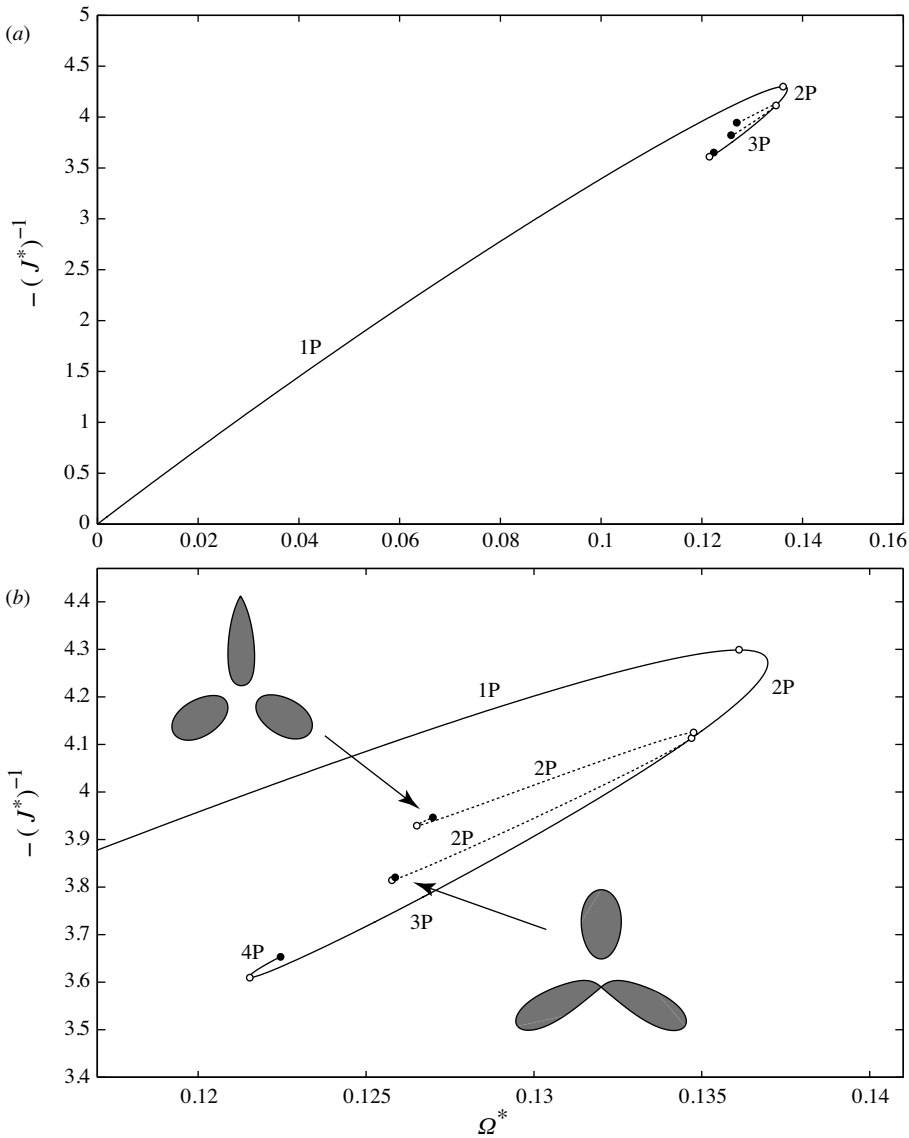

Figure 10.6. *Velocity-impulse diagram showing the entirety of the two new solution branches, discovered by using imperfections*

10.4.7. *An approximate prediction for resonance*

We apply the model of Moore and Saffman [MOO 71] to estimate eigenvalues (the details of this calculation are reported in [LUZ 11b]). Figure 10.7 shows selected

eigenvalues, plotted against $-(J^*)^{-1}$. The perturbation has the form $e^{\sigma t}$, such that a purely imaginary eigenvalue (shown as a continuous line) indicates spectral stability, whereas a real part (shown as a dashed line) implies instability. We use the energy signatures reported in section 10.4.2 to label the curves accordingly. The first intersection between opposite-signature modes is at $-(J^*)^{-1} = 4.250$, before the first turning point in impulse.

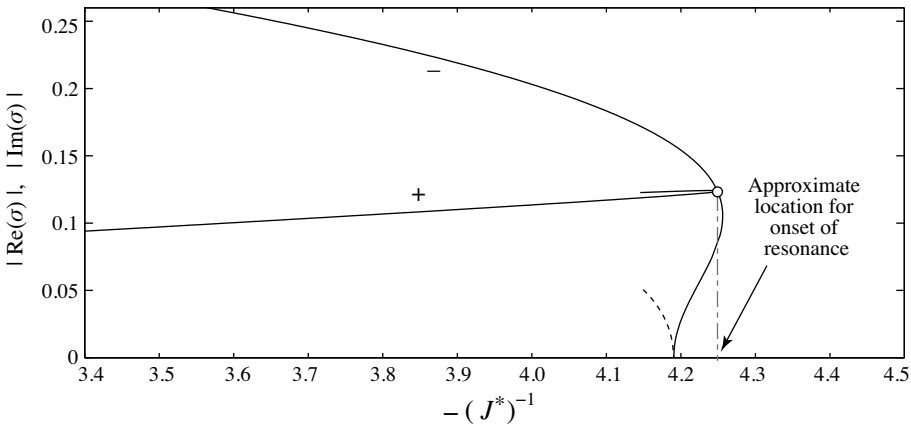

Figure 10.7. *Approximate eigenvalue plot for three vortices, used to estimate the value of J^* for the onset of resonance*

10.5. Comparison with exact eigenvalues and discussion

As a check of the energy-based stability predictions presented above, we separately performed a detailed linear stability analysis. (The numerical method used is described in [LUZ 11a].) This is the first comparison, for this flow, between exact eigenvalues and results from an IVI diagram. To facilitate this comparison, we plot selected eigenvalues versus $-(J^*)^{-1}$ in Figure 10.8. The mode signatures are also labeled. To help parse these plots, the eigenvalues are displayed incrementally, as the solution family is traversed.

Figure 10.8(a) shows eigenvalues before the first turning point in impulse. We see that linear stability is first lost through a resonance at $-(J^*)^{-1} = 4.109$, before the first turning point in impulse. This value is within 3.5% of the prediction from the approximate model. At this stage, there is one linearly unstable eigenmode, and one positive-energy mode.

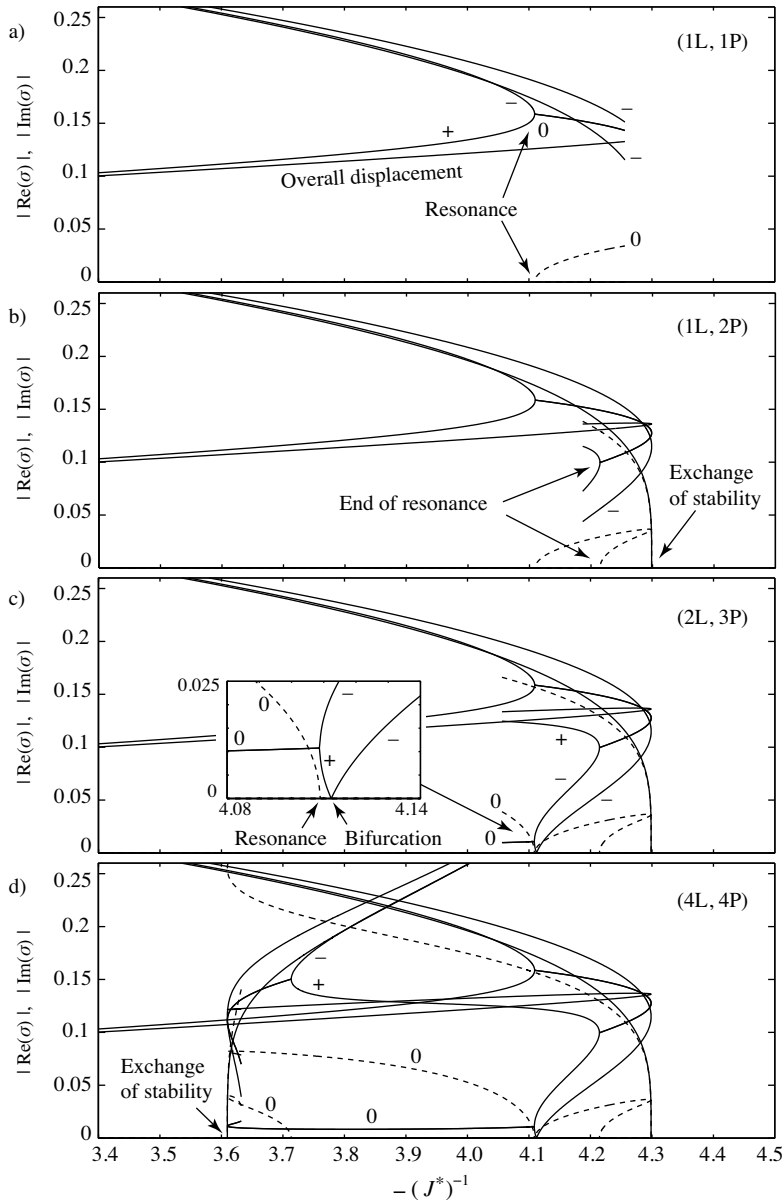

Figure 10.8. *Detailed eigenvalue plot. To ease comparison with the IVI diagram, eigenvalues are displayed in increments. In the top-right of each subplot is shown the number of linearly unstable eigenmodes, together with the number of positive-energy modes*

Figure 10.8(b) shows the eigenvalues around the first turning point in impulse. The resonance that started in Figure 10.8(a) ends after the turning point. At this stage, it is not possible to determine the signature of the separate modes that emerged from the resonance. We also note that an exchange of stability takes place at the turning point in impulse, such that the flow now has one linearly unstable eigenmode, and two positive-energy modes.

Figure 10.8(c) shows a remarkable amount of detail. At the bifurcation (which was described in section 10.4.6), one imaginary eigenvalue touches the $\sigma = 0$ axis; afterward, this eigenvalue returns to having a non-zero imaginary part, as shown in the close-up in Figure 10.8(c). From the IVI diagram of Figure 10.5, we know that at this bifurcation, a positive-signature mode is introduced. Therefore, we can infer that this eigenmode switched from a negative signature to a positive signature. The close-up in Figure 10.8(c) shows that this positive-signature eigenmode interacts with one of the eigenmodes that had emerged from the earlier resonance. Therefore, the latter eigenmode must have negative signature. At this stage, the flow has two linearly unstable eigenmodes, and three positive-energy modes.

As we continue further along the family of solutions, another resonance takes place, as shown in Figure 10.8(d). The resonant instability that began in Figure 10.8(c) is still continuing. In addition, another exchange of stability takes place at the second turning point in impulse, yielding four linearly unstable eigenmodes, and four positive-energy modes.

Finally, we note that the number of linearly unstable eigenmodes is always less than, or equal to, the number of positive-energy modes that we calculated using the IVI diagram methodology. Therefore, the linear stability results are consistent with the conclusions obtained from an IVI diagram. In addition, all instances involving a zero eigenvalue correspond to either a turning point in impulse, or to a bifurcation that we found in section 10.4.4. Therefore, all bifurcations were successfully detected by the IVI diagram methodology.

10.6. Conclusions

In this chapter, we highlight two recent approaches to infer stability information for families of equilibrium vortices. These methodologies are illustrated by means of an example involving three corotating vortices.

The first approach is based on the construction of a particular bifurcation diagram, involving the phase velocity and impulse of the array. Provided that the family of solutions is built from isovortical rearrangements, turning points in impulse correspond to a change in the number of positive-energy modes. Furthermore,

whether the change involves the introduction or removal of a positive-energy mode can be inferred from the shape of a fold in the velocity-impulse plot.

To detect hitherto undiscovered bifurcations, we introduce weak imperfections that break all geometric symmetries in the vorticity distribution, and compute the resulting families of imperfect equilibria. We find that this uncovers two new solution branches, which lead to steady states with lower symmetry.

We explicitly compute eigenvalues, eigenmodes and signatures for three well-separated vortices. By also examining the turning points in impulse for the imperfect branches, we can determine the number of positive-energy modes for each equilibrium flow.

To obtain a prediction for the onset of resonance, we calculate approximate eigenvalues using an elliptical vortex model. We then combine these with signature information, and seek eigenvalue collisions that have the potential to yield a resonance.

Finally, we compare these predictions with the results of a linear stability analysis. We verify that the number of spectrally unstable modes is always less than, or equal to, the number of positive-signature modes computed from the IVI diagram. Furthermore, it appears that the use of imperfections successfully detects all bifurcations.

10.7. Bibliography

[ARE 83] AREF H., "Integrable, chaotic, and turbulent vortex motion in two-dimensional flows", *Annual Review of Fluid Mechanics*, vol. 15, pp. 345–389, 1983.

[ARE 09] AREF H., "Stability of relative equilibria of three vortices", *Physics of Fluids*, vol. 21, p. 094101, 2009.

[BAT 56] BATCHELOR G.K., "On steady laminar flow with closed streamlines at large reynolds number", *Journal of Fluid Mechanics*, vol. 1, pp. 177–68, 1956.

[BAT 67] BATCHELOR G.K., *An Introduction to Fluid Dynamics*, Cambridge University Press, 1967.

[CAR 01] CARTON X.J., "Hydrodynamical modeling of oceanic vortices", *Surveys in Geophysics*, vol. 22, pp. 179–263, 2001.

[CRA 85] CRAIK A.D., *Wave Interactions and Fluid Flows*, Cambridge University Press, 1985.

[DAB 09] DABIRI J.O., "Optimal vortex formation as a unifying principle in biological propulsion", *Annual Review of Fluid Mechanics*, vol. 41, pp. 17–33, 2009.

[DAV 98] DAVIDSON P., "On the application of the Kelvin-Arnol'd energy principle to the stability of forced two-dimensional inviscid flows", *Journal of Fluid Mechanics*, vol. 356, pp. 221–257, 1998.

[DRA 70] DRAZIN P.G., "Kelvin-Helmholtz instability of finite amplitude", *Journal of Fluid Mechanics*, vol. 42, pp. 321–335, 1970.

[DRA 81] DRAZIN P.G., REID, W.H., *Hydrodynamic Stability*, Cambridge University Press, 1981.

[DRI 85] DRITSCHEL D.G., "The stability and energetics of corotating uniform vortices", *Journal of Fluid Mechanics*, vol. 157, pp. 95–134, 1985.

[DRI 95] DRITSCHEL D.G., "A general theory for two-dimensional vortex interactions", *Journal of Fluid Mechanics*, vol. 293, pp. 269–303, 1995.

[ELC 05] ELCRAT A., FORNBERG B., MILLER K., "Stability of vortices in equilibrium with a cylinder", *Journal of Fluid Mechanics*, vol. 544, pp. 53–68, 2005.

[FLI 11] FLIERL G.R., MORRISON P.J., "Hamiltonian-dirac simulated annealing: application to the calculation of vortex states", *Physica D*, vol. 240, pp. 212–232, 2011.

[FUK 03] FUKUMOTO Y., "The three-dimensional instability of a strained vortex tube revisited", *Journal of Fluid Mechanics*, vol. 493, pp. 287–318, 2003.

[FUK 08] FUKUMOTO Y., MOFFATT H.K., "Kinematic variational principle for motion of vortex rings", *Physica D*, vol. 237, pp. 2210–2217, 2008.

[HAV 31] HAVELOCK H., "The stability of motion of rectilinear vortices in ring formation", *Philosophical Magazine*, vol. 11, pp. 617–633, 1931.

[HOL 85] HOLM D., MARSDEN J.E., RATIU T., *et al.*, "Nonlinear stability of fluid and plasma equilibria", *Physics Reports*, vol. 123, pp. 1–116, 1985.

[KAM 87] KAMM J.R., Shape and stability of two-dimensional uniform vorticity regions, PhD Thesis, California Institute of Technology, Pasadena, CA, 1987.

[LAM 98] LAMB J., ROBERTS, J.A.G., "Time-reversal symmetry in dynamical systems: a survey", *Physica D*, vol. 112, pp. 1–39, 1998.

[LE 02] LE DIZÈS S., VERGA, A., "Viscous interactions of two co-rotating vortices before merging", *Journal of Fluid Mechanics*, vol. 467, pp. 389–410, 2002.

[LUZ 10] LUZZATTO-FEGIZ P., WILLIAMSON C.H.K., "Stability of elliptical vortices from 'Imperfect-Velocity-Impulse' diagrams", *Theoretical and Computational Fluid Dynamics*, vol. 24, pp. 181–188, 2010.

[LUZ 11a] LUZZATTO-FEGIZ P., WILLIAMSON C.H.K., "An accurate and efficient method for computing uniform vortices", *Journal of Computational Physics*, vol. 230, pp. 6495–6511, 2011.

[LUZ 11b] LUZZATTO-FEGIZ P., WILLIAMSON C.H.K., "Resonant instability in two-dimensional vortex arrays", *Proceedings of the Royal Society A*, vol. 467, pp. 1164–1185, 2011.

[LUZ 12a] LUZZATTO-FEGIZ P., WILLIAMSON C.H.K., "Determining the stability of steady two-dimensional flows through imperfect velocity-impulse diagrams", *Journal of Fluid Mechanics*, vol. 706, pp. 323–350, 2012.

[LUZ 12b] LUZZATTO-FEGIZ P., WILLIAMSON C.H.K., "Structure and stability of the finite-area von Kármán street", *Physics of Fluids*, vol. 24, 066602, 2012.

[MAD 87] MADDOCKS J.H., "Stability and folds", *Archive for Rational Mechanics and Analysis*, vol. 99, pp. 301–328, 1987.

[MEI 84] MEIRON D.I., SAFFMAN P.G., SCHATZMAN J.C., "The linear two-dimensional stability of inviscid vortex streets of finite-cored vortices", *Journal of Fluid Mechanics*, vol. 147, pp. 187–212, 1984.

[MOF 85] MOFFATT H.K., "Magnetostatic equilibria and analogous Euler flows of arbitrarily complex topology. Part 1. Fundamentals", *Journal of Fluid Mechanics*, vol. 159, pp. 359–378, 1985.

[MOO 71] MOORE D.W., SAFFMAN P.G., "Structure of a line vortex in an imposed strain" in OLSEN J.H., GOLDBURG A., ROGERS M. (eds), *Aircraft Wake Turbulence*, Plenum, pp. 339–354, 1971.

[PIE 82] PIERREHUMBERT R.T., WIDNALL S.E., "The two- and three-dimensional instabilities of a spatially periodic shear layer", *Journal of Fluid Mechanics*, vol. 114, pp. 59–82, 1982.

[SAF 80] SAFFMAN P.G., SZETO R., "Equilibrium shapes of a pair of equal uniform vortices", *Physics of Fluids*, vol. 23, pp. 2339–2342, 1980.

[SAF 82] SAFFMAN P.G., TANVEER S., "The touching pair of equal and opposite uniform vortices", *Physics of Fluids*, vol. 25, pp. 1929–1930, 1982.

[SAF 92] SAFFMAN P.G., *Vortex Dynamics*, Cambridge University Press, Cambridge, 1992.

[THO 80] THOMSON W., "Vibrations of a columnar vortex", *Proceedings of the Royal Society of Edinburg*, vol. 10, pp. 443–450. Also *Philosophical Magazine* 1880, vol. 10, pp. 155–168, 1880.